

# Modeling wheel-induced rutting in soils: Indentation

J.P. Hambleton<sup>a</sup>, A. Drescher<sup>a,\*</sup>

<sup>a</sup> Department of Civil Engineering, University of Minnesota, 500 Pillsbury Drive SE,  
Minneapolis, MN 55455, USA

## Abstract

The analysis of indentation of rigid cylindrical wheels into frictional/cohesive soils is presented. Three- and two-dimensional numerical simulations were performed using the finite element code ABAQUS to assess the influence of soil strength parameters, dilatancy, and wheel geometry on the relationship between the indentation force and wheel sinkage. The effect of three-dimensionality in the indentation process is studied in detail. Three-dimensional effects were found to be minor for clays though significant for sands. An approximate analytic approach is also presented, which relates indentation force and wheel sinkage for given wheel geometry and material parameters. Theoretical results are compared with preliminary experimental data obtained from small-scale indentation tests, and satisfactory qualitative agreement is shown. The results described in the paper are regarded as reference for numerical and analytic modeling of wheel rolling, to be presented in a separate paper.

*Keywords:* Rigid wheel indentation; Finite element method; Elastic-plastic; Analytic; Experiments; PIV; Clay; Sand

---

\* Corresponding author. Tel.: +1-612-625-2374; fax: +1-612-626-7750.

*E-mail addresses:* dresc001@umn.edu (A. Drescher), hamb0025@umn.edu (J.P. Hambleton).

## 1. Introduction

Hauling trucks, off-road recreational vehicles, and special purpose vehicles often induce permanent wheel impressions, or ruts, in soils. Negative implications of rutting include destruction of vegetation and erosion [1] in sensitive natural areas such as parks, forests, and wetlands. When viewed in a positive light, a soil's susceptibility to rutting can be understood as an indicator of its strength, and novel test methods for determining *in situ* soil strength parameters can be premised on measurement of rut depth [2]. Accurate prediction of rutting is central in both assessing land damage and relating rut depth to soil strength.

A rut is a manifestation of inelastic deformation and results from the loading/unloading process present with a rolling wheel. Rut formation begins when the wheel first encounters soil prone to rutting, e.g., rolls from a stronger material onto a weaker one. The initial phase of rut formation is rather complex but bears similarity to the simpler process of wheel indentation, in which a wheel displaces normally into the soil without translation or rotation. Indentation is directly involved when stationary vehicles are loaded gradually or lowered onto the soil.

This paper deals with modeling wheel indentation as a quasi-static process. The approach and the results presented are viewed as reference for modeling rut formation during wheel rolling, to be presented in a separate paper. The motivation for considering indentation and rolling separately derives from crucial differences in the two processes affecting the analysis. Indentation is a continuous loading process with a growing region of deformation, whereas in rolling there is a loading/unloading sequence and deformation

at an advanced state can be steady in time. Also, wheel indentation is characterized by double symmetry in the deformation field (parallel and perpendicular to the plane of the wheel) as opposed to single symmetry in the case of rolling (parallel to the plane of the wheel).

The approaches discussed in this paper are based on preliminary findings by Hambleton [2] and Hambleton and Drescher [3] related to modeling test rolling, a procedure used in roadway embankment construction for quality assurance. In these works, theoretical models were formulated to expand on existing empirical, analytic, and numerical approaches for modeling soil-wheel interaction, which are amply illustrated in the literature and summarized, for example, in books by Bekker [4], Karafiath and Nowatzki [5], and Wong [6].

The analysis of shallow indentation of objects into a stratum constitutes one of the main topics of contact mechanics (cf. [7]), with the results used extensively in evaluating mechanical properties of metals as well as polymeric coatings (microindentation). Such analyses were considered by Bishop *et al.* [8], Mulhearn [9], Lawn and Marshall [10], Yu and Blanchard [11], Mesarovic and Fleck [12], Da Silva Botelho *et al.* [13], Kucharski and Mroz [14], and numerous others. Various analysis techniques and material models have been employed. Analytic or semi-analytic solutions are possible for plane or axisymmetric objects and simplified material models, examples being wedge indentation into metals [15] and soils [16,17] and indentation of pyramids or cones into rocks [18-21]. In some of these papers, self-similarity of the solution was postulated, which makes the analysis much simpler. However, wheel indentation is inherently non-similar as the material displaced by the indenter is in contact with a surface of varying local inclination.

Also, neither a plane mode nor an axisymmetric mode of deformation accurately describes the process.

A viable tool for obtaining solutions to geometrically complex problems is the finite element method, which has been used increasingly in recent years to study soil-object interaction [22-25]. In contrast to wheel rolling [23-25], however, references dealing specifically with numerical simulations of wheel indentation into soils appear to be missing. While some work on two-dimensional simulations of punch indentation in metals [26] can be used as reference for indentation in clays, three-dimensional analyses for frictional/cohesive soils are missing from the literature altogether. For this paper, numerical simulations using the finite element code ABAQUS were performed to gain an understanding of the influence of essential soil properties and wheel geometry on the indentation process. In particular, the effect of three-dimensionality in wheel indentation was assessed through simulation of varying wheel geometries and comparison with two-dimensional (plane strain) simulations.

In numerical simulations, the soil was modeled as an elastic-perfectly plastic cohesive/frictional material obeying the Mohr-Coulomb yield condition and associated or non-associated plastic flow. Such an elastic-plastic model for the soil has been widely used in solving geomechanics problems and often serves as reference for more sophisticated models. Although it is an approximation of the true soil response, this model captures the essential recoverable and permanent parts of deformation and contains a minimal number of parameters (two elastic: Young's modulus  $E$  and Poisson's ratio  $\nu$ ; three plastic: friction angle  $\phi$ , cohesion  $c$ , and dilation angle  $\psi \leq \phi$ ), thus making it possible to evaluate material parameters from a limited number of well-established

tests. As the yield condition in the model does not possess a cap, focus is on indentation into soils with limited ability to compact, i.e., soils for which the compaction state (density) is reflected in the magnitude of parameters.

The soil model selected also makes it possible to compare the numerical results with results of an approximate analytic approach in which soil elastic properties and dilatancy are disregarded. In fact, selecting a large Young's modulus in the elastic-plastic model closely approximates the rigid-plastic one. As preliminary findings demonstrate [2,3], the analytic approach yields useful formulas that may be easily applied in practical applications. In this paper, the analytic approach presented in [2,3] for purely cohesive soil ( $\varphi = 0$ ) is extended to frictional ( $c = 0$ ) and frictional/cohesive ( $\varphi, c \neq 0$ ) materials.

In both the numerical and analytic approaches, the geometry of the wheel is simplified to a right cylindrical shape with no local irregularities, and the wheel is assumed to be rigid. This assumption has proven successful in some previous works (cf. [4,5]). Indentation of flexible as well as toroidal wheels will be discussed elsewhere.

Finally, to assess the adequacy of the theoretical approaches and the soil models selected, the results are compared with exploratory small-scale wheel indentation experiments performed on granular and cohesive soils.

## **2. Numerical simulations**

Numerical simulations were performed using the finite element code ABAQUS/Explicit. This particular software, unlike many other commercial codes, has the option of using an Arbitrary Lagrangian-Eulerian (ALE) mixed formulation, which

makes remeshing possible in the case of large deformations. While remeshing is not required for simulating wheel indentation, it is a virtual requisite for successful modeling of rolling processes. ABAQUS/Explicit performs fully dynamic analysis, though it readily recovers a quasi-static solution when boundary conditions are smoothly applied and the process is simulated over sufficiently large time.

In ABAQUS/Explicit, the Mohr-Coulomb yield condition (pyramid with edges) is approximated by a modified Drucker-Prager yield condition [27] with a corresponding associated or non-associated flow potential. The Drucker-Prager condition was implemented by exactly matching the Mohr-Coulomb condition in triaxial compression, while matching as closely as possible in triaxial extension. A limitation inherent in the code pertains to the selection of the plastic parameters  $\varphi$  and  $c$ . Whereas meaningful results could be obtained for soils with  $\varphi \geq 0$  and  $c > 0$ , numerical instabilities prevented considering a purely frictional material ( $\varphi > 0$  and  $c = 0$ ). For this reason, very small cohesion was used when simulating sand. Three-dimensional simulations with large  $\varphi$  and an associated flow rule ( $\psi = \varphi$ ) were also found to be generally unstable as a result of extreme volumetric strains. As focus was directed at the effects of soil strength and dilatancy, elastic properties were fixed at  $E/\gamma d = 1000$  and  $\nu = 0.3$  in all simulations, where soil unit weight  $\gamma$  and wheel diameter  $d$  are used for normalization.

The reference configuration used for simulating three-dimensional indentation is shown in Fig. 1. The same mesh in the  $x$ - $z$  plane was used in two-dimensional (plane strain) simulations. The soil was discretized using linear, 8-node, reduced integration, hexahedral elements (4-node, rectangular elements for plane strain) with hourglass control. The total number of elements was 48,000 for the three-dimensional simulations

and 1,200 with plane strain. Out-of-plane displacements were not allowed on all surfaces except the free surface in the  $x$ - $y$  plane, thereby incorporating the symmetry conditions in the  $x$ - $z$  and  $y$ - $z$  planes and allowing some freedom at remaining boundaries. These remaining boundaries were located far enough from the wheel that their effects were negligible. The right-cylindrical wheel of diameter  $d$  and width  $b$  was modeled as an analytical rigid surface, meaning that it was smooth within the computational precision of the code (i.e., not discretized) and governed by a single reference node. The wheel possessed an edge fillet with a radius taken as a small fraction of the wheel width. A non-zero fillet radius was required to avoid numerical problems arising from the algorithm used to model contact between the wheel and the soil. Dry friction with coefficient of friction  $\mu$  controlled contact interaction between the wheel and soil. Except where specified otherwise, the coefficient of friction was  $\mu = 0.5$  in the simulations.

Simulation consisted of first applying unit weight to the soil in the form of a uniform body force and then displacing the wheel vertically into the soil at a specified velocity. The wheel penetration depth referenced from the undisturbed soil surface is referred to as sinkage and denoted  $s$ .

Force-sinkage curves resulting from simulation are presented through the dimensionless variables  $Q/\gamma b d^2$  and  $s/d$ . It should be noted that total force  $Q$  and wheel width  $b$  are not defined in plane strain. Rather, force per unit width  $Q^*$  is the operative variable in plain strain and the corresponding dimensionless variable is  $Q^*/\gamma d^2$ . The force  $Q^*$  can be understood as the ratio  $Q/b$  in the limit where the wheel aspect ratio  $b/d$  goes to infinity, and for notational simplicity,  $Q^*$  and  $Q/b$  are taken to have the same meaning in plane strain.

### 3. Results of numerical simulations

The force-sinkage relationship for several values of  $b/d$  is shown in Fig. 2 for a purely cohesive, nearly incompressible soil ( $c/\gamma d = 1.25$ ,  $\phi = \psi = 0$ ) such as saturated clay. The undulations in the curves are algorithmic, as the nodal points come in contact with the wheel at intervals. Increasing the number of elements reduces this effect without shifting the overall curves, and within the intervals the smoothness of the response indicates robustness and stability of the algorithm. Overall, force increases with sinkage with decreasing rate, and the effect of  $b/d$  is relatively small, with normalized force increasing slightly with decreasing  $b/d$ .

Qualitatively different results were obtained from indentation in sand, and they strongly depend on the dilation angle  $\psi \leq \phi$  (non-associativity). Fig. 3 illustrates the extent of the deformed region of soil when  $\psi$  is varied from  $\psi = 0$  to  $\psi = \phi/3$  for a sand-type soil and  $b/d = 0.3$ . With increasing  $\psi$ , the volume of the deformed region and the contact area increase. This is the consequence of a constitutive model for the soil that assumes constant dilation angle. The influence of  $\psi$  is also visible as a significant increase in the indentation force (Fig. 4). For large  $\psi$ , excessively large volumetric strains give rise to instabilities that cause termination of the simulation.

In contrast to the nonlinear force-sinkage curves observed for clay, force is a nearly linear function of sinkage for sand. Also, the wheel aspect ratio  $b/d$  has greater effect in sand than for clay, as illustrated in Figs. 5-7 for several different  $\phi$  and  $\psi = 0$ . For small values of  $\phi$ , wide wheels yield the highest force (per unit width), whereas for large  $\phi$  the highest force corresponds to a particular aspect ratio away from small or large  $b/d$ .



Despite the apparent instabilities present in some of the simulations, especially those corresponding to large  $\phi$ , the indentation force clearly displays dependence on  $b/d$ .

Results from numerical simulations for soils with both cohesion and internal friction are shown in Fig. 8 for  $b/d = 0.3$ . As expected, the indentation force increases as a result of an increase in either  $c$  or  $\phi$ . Cohesion increases indentation force at a slightly decreasing rate, while internal friction increases indentation force at an increasing rate (roughly exponentially).

The coefficient of interface friction  $\mu$  was found to have relatively little influence on the computed indentation force (Fig. 9). For clay, the effect of varying  $\mu$  from 0.1 to 10 is barely noticeable. For sand, the change in indentation force is more pronounced.

The numerical simulations are case-specific, and from the outset there is no clear way to encapsulate such results in a tractable formula. The next section presents an analytic approach that provides algebraic formulas in support of the findings from the numerical simulations.

#### **4. Approximate analytic approach**

The approximate analytic approach originating from the work of Hambleton [2] and Hambleton and Drescher [3] hinges on an assumption that the soil can be modeled as rigid-perfectly plastic Mohr-Coulomb material (i.e., the elastic deformations are disregarded). It is further postulated that the continuous process of indentation can be decomposed into a sequence of states and the resulting process response constructed. The last assumption is that each indentation step is analogous to the plastic state beneath a

rigid shallow foundation (punch). This assumption is supported by the results of numerical simulation of wheel indentation shown in Fig. 10a, which depicts the velocity field obtained under plane strain conditions for a soil with  $\varphi = 0$ . This velocity field is nearly identical to the one obtained by Prandtl [28] for a flat strip footing with the same width as the contact length between the wheel and soil, acting on a rigid-plastic half plane (Fig. 10b). Thus, if penetration of the wheel is small in relation to wheel's diameter, considering the contact area of the wheel (which grows with increasing  $s$ ) as a flat surface seems acceptable. As Prandtl's solution is the basis of Meyerhof's bearing capacity formula [29] for plane and rectangular footings (a generalization of the Terzaghi's formula [30]), average stress over the soil-wheel contact area can be calculated semi-analytically for each indentation step. In using Meyerhof's formula, the full three-dimensionality of the indentation process is preserved.

Some bearing capacity concepts have been utilized previously in studying soil-wheel interaction (cf. [31,32]), although their use in these works appears in the context of semi-empirical methods [4]. In the present approach, the global force-sinkage response is formulated by means of a direct analogy between bearing capacity and wheel indentation.

Meyerhof's formula for bearing capacity  $q_u$ , the average vertical stress at the footing/soil interface, is

$$q_u = cN_c F_{cs} F_{cd} + qN_q F_{qs} F_{qd} + \frac{1}{2} \gamma B N_\gamma F_{\gamma s} F_{\gamma d} \quad (1)$$

where  $N_c \dots$  are factors depending on  $\varphi$ ,  $F_{cs} \dots$  are factors depending on the footing width  $B$  and length  $L$  ( $B \leq L$ ),  $F_{cd} \dots$  are factors depending on the footing depth  $D$ , and  $q = \gamma D$  is

the surcharge acting at the depth  $D$ . Eq. (1) is derived from static considerations without any account for the flow rule and therefore does not depend on the dilation angle  $\psi$ . From the average stress  $q_u$  and the contact area  $BL$ , the total force  $Q$  acting on the footing is

$$Q = q_u BL \quad (2)$$

Expressions for the various factors in Eq. (1) used in foundation design are given in the Appendix. Alternatively, the results of numerical simulations could be used to derive new expressions. As the latter would require extensive numerical simulations and Eq. (1) is approximate (assumes superposition of cohesion, surcharge and weight effects), the formulas used in foundation design were implemented, and the resulting predictions were compared with numerical simulations.

Fig. 11 illustrates indentation of a cylindrical rigid wheel. The length of the contact area  $h$  is taken as the length of a chord intersecting the indented wheel at the initial soil level. This gives the expression

$$h = 2\sqrt{ds - s^2} \quad (3)$$

The validity of Eq. (3), postulated *ad hoc* by Hambleton [2], was assessed using the results of numerical simulations. From Fig. 12, it is evident that Eq. (3) tends to somewhat underestimate the contact length. One conceivably could determine an improved expression for  $h$  that accounts for  $c$ ,  $\phi$ , and  $\psi$ , but Eq. (3) suffices as a first approximation. The equivalent foundation width and length for an indenting wheel are

$$\left. \begin{array}{l} B = h \\ L = b \end{array} \right\} \text{ for } h < b; \quad \left. \begin{array}{l} B = b \\ L = h \end{array} \right\} \text{ for } h \geq b \quad (4)$$

An indenting wheel displaces material above the original soil surface. To account for this material as surcharge  $q$  and through the depth factors  $F_{cd}...$  in Eq. (1), mass balance of soil displaced by the wheel is used. Prandtl's plasticity solution is the basis of Eq. (1), and from this solution it is possible to estimate the equivalent depth  $D$ . Approximating the displaced volume of soil by the rectangular prisms shown in Fig. 11 and equating it to the volume occupied by the wheel (see [2] for detailed derivation) gives

$$D \approx \frac{1}{6} s \quad (5)$$

Eq. (5) was derived assuming incompressibility, which holds for saturated clays and non-associated ( $\psi = 0$ ) sands. Combining Eqs. (1-5) gives algebraic expressions (Appendix) relating indentation force to sinkage.

Fig. 13 compares the force-sinkage relationship for clay obtained using the analytic approach with the predictions determined through numerical simulation. The analytic prediction shows the same nonlinear trend as the numerical simulations, and quantitative agreement is satisfactory for small sinkage. At high sinkage, the analytic prediction underestimates the numerical results. This underestimation is in large part because the contact length is underestimated in the analytic method (Fig. 12). The predictions using the analytic approach do not quantitatively predict the effect of  $b/d$ , however the approach captures the insensitivity of indentation force to  $b/d$ .

For sand (Figs. 14 and 15), differences in the predictions based on the analytic approach and the numerical simulations are large for some cases and small for others. Especially for large  $\varphi$  (Fig. 15), the increase in force resulting from an increase in  $\psi$  is quite dramatic. This dependence on  $\psi$ , present exclusively in the numerical simulations, makes comparison of the two approaches rather ambiguous. Nonetheless, the two approaches again provide qualitatively similar predictions

## 5. Small-scale experiments

Small-scale tests were conducted to investigate the deformation field beneath a wheel indenting a granular material. In particular, the extent of the deformation field related to dilatancy and the possible presence of localized deformation (shear bands) were of interest. The occurrence of multiple periodic shear bands in sands is known in plane wedge indentation [33], although no experiments exploring the presence of shear bands in wheel indentation were previously performed.

A container of length 780 mm, height 440 mm, and width 80 mm with a Plexiglas front wall was filled to a depth of 250 mm with crushed walnut shells, a material closely resembling sand but less abrasive against the Plexiglas wall [34]. The material was rained into the top of the container through a scattering device and compacted in 30 mm lifts to a density of  $730 \text{ kg/m}^3$ . The friction angle of the material determined from triaxial compression tests ranged from  $\varphi = 41^\circ$  at low confining pressure to  $\varphi = 38^\circ$  at higher pressures. A nylon wheel with diameter  $d = 100 \text{ mm}$  and width  $b = 19 \text{ mm}$  was placed flush with the transparent wall and indented vertically, thus inducing approximately one

half of three-dimensional indentation ( $b/d = 0.38$ ). The surface of the wheel in contact with the walnut shells was covered in coarse sand paper to replicate high friction. Friction between the particles and the transparent wall distorted the deformation field somewhat, but its main characteristics were preserved. Digital photographs were taken at various stages of indentation, and they were processed using PIV software to extract the field of incremental displacements [35].

Figs. 16 and 17 show the increments of displacements from indenting a densely packed material with two wheels: one as described ( $b/d = 0.38$ ) and one with the same width as the container (plane strain). For  $b/d = 0.38$  and small  $s$  (Fig. 16a), the deforming region increases as  $s$  increases, but as  $s$  becomes large (Fig. 17a), material moves predominantly to the side of the wheel and the deforming region at the wheel midplane does not grow significantly. Furthermore, the deforming region is not bounded by a strong discontinuity in incremental displacement (shear band). In plane strain, a distinct boundary occurs at larger sinkage (Fig. 17b). The absence of shear bands for  $b/d = 0.38$  can be interpreted as the effect of three-dimensionality, which suppresses shear band formation. In fact, it has been shown theoretically that plane strain is more prone to deformation localization than axisymmetry [36,37]. In either case, the deformation field closely resembles that from numerical simulations with average friction angle  $\varphi = 40^\circ$  and dilation angle  $\psi = 20^\circ$ , as illustrated in Fig. 16.

Fully three-dimensional small-scale experiments were also conducted to determine the relationship between indentation force and sinkage. An aluminum wheel with coarse sandpaper adhered to the cylindrical surface was used. Dimensions of the wheel were  $d = 115$  mm and  $b = 38$  mm. A load cell and an LVDT were used to measure indentation

force and sinkage as the wheel was indented with constant velocity (0.1 mm/s) into the center of a soil-filled container [2]. The container had depth 100 mm, width 250 mm, and length 300 mm.

Tests were conducted on two soils, one cohesive and the other frictional. A Minnesota clay [38] was crushed and combined with water in a mixer to obtain a water content of 37%. Uniaxial and triaxial compression tests revealed a uniaxial compression yield strength  $\sigma_o = 2c = 57.7$  kPa and friction angle  $\phi \approx 3^\circ$ . The Young's modulus determined from the initial portion of the uniaxial compression stress-strain curve was  $E = 2$  MPa. A well-graded sand [39] was tested in a dense state corresponding to a density of  $1770$  kg/m<sup>3</sup>. Triaxial compression tests revealed a nonlinear failure envelope for this sand at low stress levels, with the friction angle varying from  $\phi = 42^\circ$  to  $\phi = 46^\circ$ . A Young's modulus of approximately  $E = 20$  MPa was found from triaxial tests.

Figs. 18 and 19 depict the measured force-sinkage curves in comparison with curves from numerical simulations and the analytic method. The agreement for clay is very good, with the analytic method somewhat overestimating the indentation force at low sinkage (underestimating sinkage at low force) as a result of neglected elastic effects. For sand, the agreement between the experimental results and the prediction using the analytic approach is excellent. The overestimation of indentation force from the numerical simulation in Fig. 19 can be attributed in part to the presence of the cohesion necessary for a stable solution. The results of simulation with  $c/\gamma d = 5 \times 10^{-4}$  are noticeably more erratic but closer to the experimental data than the simulation with  $c/\gamma d = 5 \times 10^{-2}$ . Numerical results for the sand are with  $\psi = 0$ . The agreement between the numerical and experimental results would clearly be worse for  $\psi > 0$ , although  $\psi > 0$  is surely the case

for the dense sand tested. A better match could possibly be obtained by using a non-linear yield condition, but nevertheless, the comparison for both soils shows that the simple elastic-plastic model is sufficiently accurate to capture the experimentally observed force-sinkage response.

## 6. Conclusions

Two approaches, one numerical and the other approximate analytic, were applied in analyzing indentation of wheels into soils modeled as elastic-perfectly plastic or rigid-perfectly plastic materials. Numerical simulations for frictionless soils (clay) lead to force-sinkage response curves close to those obtained from small-scale experiments. For frictional soils (sand), the response curves differ somewhat from the experimental ones, although reasonable agreement is obtained if dilatancy is suppressed by selecting small  $\psi$  or even  $\psi = 0$  (plastic incompressibility). A similar result was reported previously in plane strain wedge indentation [16]. The approximate analytic approach is simple and provides a prediction comparable to the numerical and experimental results.

Both the analytic and numerical approaches predict similar influence of wheel three-dimensionality. For clays, three-dimensional effects have a small influence on the normalized (per unit width) indentation force, and the plane-strain approximation appears to be reasonable. For sands, this influence is greater and depends on the friction angle.

In the numerical approach, indentation force  $Q$  depends on ten parameters:  $s$ ,  $b$ ,  $d$ ,  $E$ ,  $\nu$ ,  $c$ ,  $\phi$ ,  $\psi$ ,  $\mu$  and  $\gamma$ . The effect of elasticity was not investigated in detail; however, as the present paper is viewed as reference for analyzing permanent rutting, the influence of



plastic rather than elastic properties seems more important. It was found in simulations that the friction coefficient  $\mu$  has a relatively insignificant effect, although  $\mu$  has some influence with frictional materials. In the analytic approach, the parameters  $E$ ,  $\nu$ ,  $\psi$  and  $\mu$  are not present. The dilation angle is the important parameter that distinguishes the numerical and analytic approaches, and its influence on the results of numerical simulations is profound.

This strong effect of  $\psi$  on indentation force appears to be somewhat contradictory to the common assessment of the influence of non-associativity in perfectly plastic models used in determining failure loads in geotechnical problems such as footings and retaining walls. It is generally agreed that in those problems non-associativity has moderate if not little effect on the failure load. The reason for this contradiction can be attributed to wheel indentation being a process characterized by continually growing contact area and deformation region, both controlled by dilatancy, whereas failure of footings or walls takes place at a particular deformation state and with predefined contact area.

In the numerical simulations, a soil constitutive model that is more sophisticated than the one used may give a much better match with experiments. However, simple models provide good reference for improvements and are of greater benefit in practical applications, where a balance must be struck between precision and tractability. An example is the approximate analytic approach, which appears to be reasonable and can be easily used for evaluating the effects of the basic soil strength parameters ( $c$  and  $\varphi$ ) and wheel geometry on the indentation force-wheel sinkage response.

## Acknowledgements

Financial support provided by the Minnesota Local Road Research Board and the Shimizu Corporation are gratefully acknowledged. Computer resources were provided by the Minnesota Supercomputing Institute.

## Appendix

Bearing capacity factors [28,40,41]:

$$N_q = \tan^2\left(\frac{\pi}{4} + \frac{\varphi}{2}\right) e^{\pi \tan \varphi}, \quad N_c = (N_q - 1) \cot \varphi, \quad N_\gamma = 2(N_q + 1) \tan \varphi$$

Shape factors [42]:

$$F_{cs} = 1 + \frac{B}{L} \frac{N_q}{N_c}, \quad F_{qs} = 1 + \frac{B}{L} \tan \varphi, \quad F_{\gamma s} = 1 - 0.4 \frac{B}{L}$$

Depth factors [43]:

$$F_{cd} = 1 + 0.4 \frac{D}{B}, \quad F_{qd} = 1 + 2 \tan \varphi (1 - \sin \varphi)^2 \frac{D}{B}, \quad F_{\gamma d} = 1 \quad \left(\frac{D}{B} \leq 1\right)$$

$$F_{cd} = 1 + 0.4 \tan^{-1}\left(\frac{D}{B}\right), \quad F_{qd} = 1 + 2 \tan \varphi (1 - \sin \varphi)^2 \tan^{-1}\left(\frac{D}{B}\right), \quad F_{\gamma d} = 1 \quad \left(\frac{D}{B} > 1\right)$$

Indentation force:

$$Q = 2b\sqrt{ds - s^2} \left\{ cN_c \left( 1 + \frac{2\sqrt{ds - s^2}}{b} \frac{N_q}{N_c} \right) \left( 1 + \frac{0.03s}{\sqrt{ds - s^2}} \right) \right. \\ \left. + 0.17\gamma s N_q \left( 1 + \frac{2\sqrt{ds - s^2}}{b} \tan \varphi \right) \left[ 1 + \frac{0.17s \tan \varphi (1 - \sin \varphi)^2}{\sqrt{ds - s^2}} \right] \right. \\ \left. + \gamma \sqrt{ds - s^2} N_\gamma \left( 1 - \frac{0.8\sqrt{ds - s^2}}{b} \right) \right\}$$

for  $2\sqrt{ds-s^2} < b$  and

$$Q = 2b\sqrt{ds-s^2} \left\{ cN_c \left( 1 + \frac{0.5b}{\sqrt{ds-s^2}} \frac{N_q}{N_c} \right) \left( 1 + \frac{0.07s}{\sqrt{ds-s^2}} \right) \right. \\ \left. + 0.17\gamma s N_q \left( 1 + \frac{0.5b}{\sqrt{ds-s^2}} \tan \varphi \right) \left[ 1 + \frac{0.33s \tan \varphi (1 - \sin \varphi)^2}{b} \right] \right. \\ \left. + \gamma b N_\gamma \left( 0.5 - \frac{0.1b}{\sqrt{ds-s^2}} \right) \right\}$$

for  $2\sqrt{ds-s^2} > b$

## References

- [1] Li Q, Ayers PD, Anderson, AB. Prediction of impacts of wheeled vehicles on terrain. *J Terramech* 2007;44(2):205-215.
- [2] Hambleton JP. Modeling test rolling in clay. MS thesis, University of Minnesota, Minneapolis; 2006.
- [3] Hambleton JP, Drescher A. Modeling test rolling on cohesive subgrades. In: Proc of the int conf on adv charact pave and soil engng mater, vol. 1, Athens, Greece; 2007. p. 359-368.
- [4] Bekker MG. Introduction to terrain-vehicle systems. Ann Arbor: University of Michigan Press; 1969.
- [5] Karafiath LL, Nowatzki EA. Soil mechanics for off-road vehicle engineering, Clausthal: Trans Tech Publications; 1978.
- [6] Wong JY. Theory of ground vehicles. New York: Wiley; 2001.
- [7] Johnson KL. Contact mechanics. Cambridge: Cambridge University Press; 1985.
- [8] Bishop RF, Hill R, Mott N. The theory of indentation and hardness tests. *Proc Phys Soc* 1945;57:47-159.
- [9] Mulhearn T. Deformation of metals by Vickers-type pyramidal indenters. *J Mech Phys Solids* 1959;7:85-96.

- [10] Lawn B, Marshall D. Hardness, toughness, and brittleness: an indentation analysis. *J Am Ceramic Soc* 1979;62(7):347–350.
- [11] Yu W, Blanchard JP. An elastic-plastic indentation model and its solutions. *J Mater Res* 1996;11(9):2358-2367.
- [12] Mesarovic SD, Fleck NA. Spherical indentation of elastic-plastic solids. *Proc Roy Soc A* 1999;455:2707-2728.
- [13] Da Silva Botelho T, Proгри R, Inglebert G, Robbe-Valloire F. Elastoplastic indentation of a layered half-space with an infinite-length cylinder. *Mech Mater* 2005;37(6):629-639.
- [14] Kucharski S, Mroz Z. Identification of yield stress and plastic hardening parameters from a spherical indentation test. *Int J Mech Sc* 2007;49(11):1238-1250.
- [15] Hill R, Lee EH, Tupper SJ. The theory of wedge indentation of ductile materials. *Proc Roy Soc A* 1947;188:273-289.
- [16] Drescher A, Kwaszczynska K, Mroz Z. Static and kinematics of the granular medium in the case of wedge indentation. *Arch Mech Stos* 1967;19:99-113.
- [17] Drescher A, Michalowski RL. Density variation in pseudo-steady plastic flow of granular media. *Geotechnique* 1984;34(1):1-10.
- [18] Michalowski RL. Limit analysis of quasi-static pyramidal indentation of rock. *Int J Rock Mech Min Sci* 1985;22(1):31-38.
- [19] Michalowski RL. An approximate solution to a problem of pseudo-steady flow of strain-hardening material. *Int J Mech Sci* 1986;28(4):195-200.
- [20] Huang H, Damjanac B, Detournay E. Normal wedge indentation in rocks with lateral confinement. *Rock Mech Rock Engng* 1998;31(2):81–94.
- [21] Alehossein H, Detournay E, Huang H. An analytical model for the indentation of rocks by blunt tools. *Rock Mech Rock Engng* 2000;33(4):267-284.
- [22] Abo-Elnor M, Hamilton R, Boyle JT. 3D Dynamic analysis of soil-tool interaction using the finite element method. *J Terramech* 2003;40(1):51-62.
- [23] Fervers CW. Improved FEM simulation model for tire-soil interaction. *J Terramech* 2004;41(2-3):87-100.
- [24] Liu CH, Wong JY. Numerical simulations of tire-soil interaction based on critical state soil mechanics. *J Terramech* 1996;33(5):209-221.

- [25] Chiroux RC, Foster WA, Johnson CE, Shoop SA, Raper RL. Three-dimensional finite element analysis of soil interaction with a rigid wheel. *Appl Math and Comp* 2005;162(2):707-722.
- [26] Cinar A, Sinclair GB. Quasi-static normal indentation of an elasto-plastic half-space by a rigid circular cylinder of infinite length. *Int J Solids Struct* 1986;22(8):919-934.
- [27] ABAQUS Version 6.6 Documentation. Providence: ABAQUS, Inc.; 2004.
- [28] Prandtl L. Über die Eindringungsfestigkeit (Härte) plastischer Baustoffe und die Festigkeit von Schneiden. *Zeit Ang Math Mech* 1921;1(1):15-20.
- [29] Meyerhof GG. Some recent research on bearing capacity of foundations. *Can Geotech J* 1963;1(1):16-26.
- [30] Terzaghi K. *Theoretical soil mechanics*. New York: Wiley; 1943.
- [31] Hetherington JG, Littleton I. The rolling resistance of towed, rigid wheels in sand. *J Terramech* 1978;15(2):95-105.
- [32] Kim KU, Shin BS. Modeling motion resistance of rigid wheels. *J Terramech* 1986;22(4):225-236.
- [33] Butterfield R, Andrawes KZ. An investigation of a plane strain continuous penetration problem. *Geotechnique* 1972;22(4):597-617.
- [34] Waters AJ, Drescher A. Modeling plug flow in bins/hoppers. *Powd Techn* 2000;113(1):168-175.
- [35] White DJ, Take WA, Bolton MD. Soil deformation measurement using particle image velocimetry (PIV) and photogrammetry. *Geotechnique* 2003;53(7):619-731.
- [36] Cox AD, Eason G, Hopkins HG. Axially symmetric plastic deformations in soils. *Roy Soc Phil Trans A* 1961;254(1036):1-45.
- [37] Vardoulakis I, Sulem J. *Bifurcation analysis in geomechanics*. London: Chapman and Hall; 1995.
- [38] Swenson JN, Guzina BB, Labuz JF, Drescher A. Moisture effects on PVD and DCP measurements. Report No MN/RC-2006-26, Minnesota Department of Transportation, Research Services Section, St. Paul; 2006.

- [39] Przeslawski PA. Characterization of granular base materials using portable vibratory deflectometer and bender element testing. MS thesis, University of Minnesota, Minneapolis; 2004.
- [40] Reissner H. Zum Erddruckproblem. In: Proc 1st int Congr appl mech, Delft, The Netherlands; 1924. p. 295-311.
- [41] Vesic AS. Analysis of ultimate loads of shallow foundations. J Soil Mech Found Div ASCE 1970;99(1):45-73.
- [42] De Beer EE. Experimental determination of the shape factors and bearing capacity factors of sand. Geotechnique 1970;20(4):387-411.
- [43] Hansen JB. A revised and extended formula for bearing capacity. Bulletin 28, Danish Geotechnical Institute, Copenhagen; 1970.

**Figures**

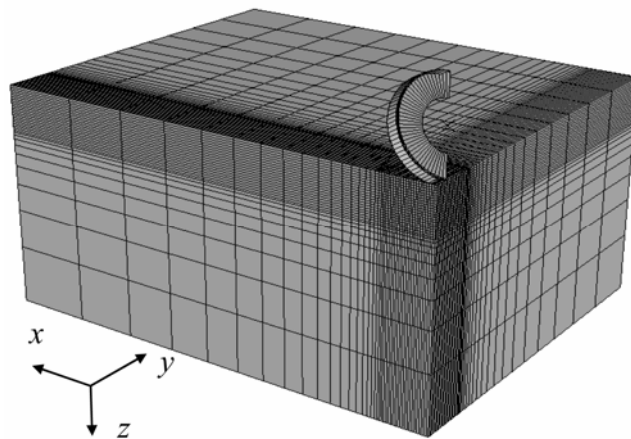


Fig. 1. Three-dimensional mesh and indenting wheel.

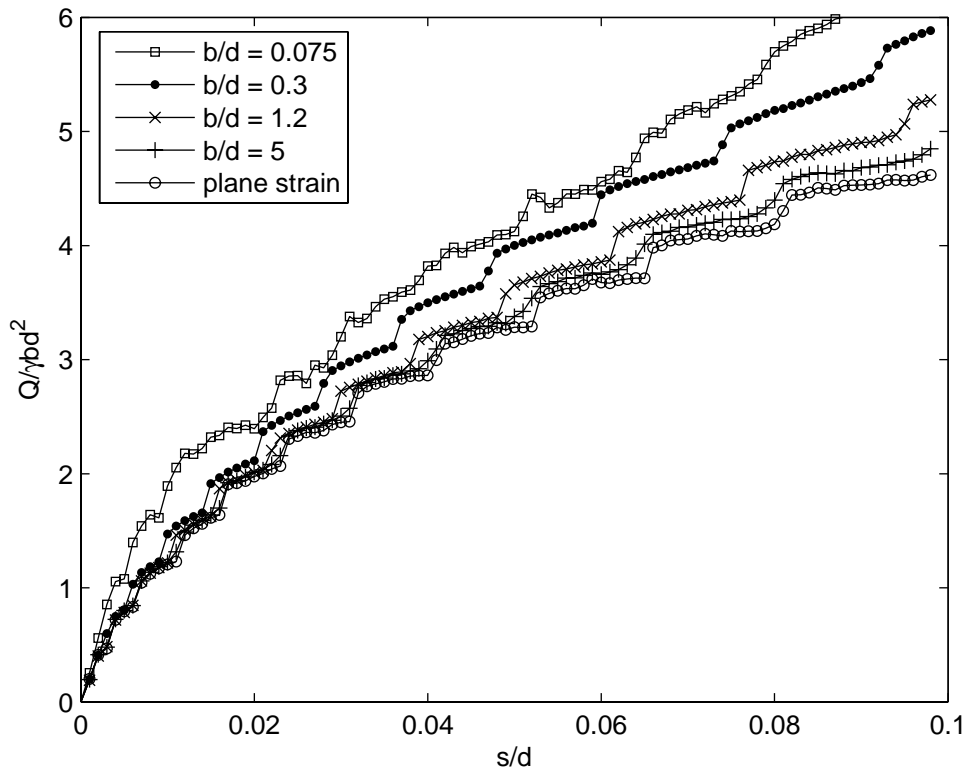


Fig. 2. Indentation force for clay soil with varying  $b/d$  ( $\varphi = 0$ ,  $c/\gamma d = 1.25$ ).

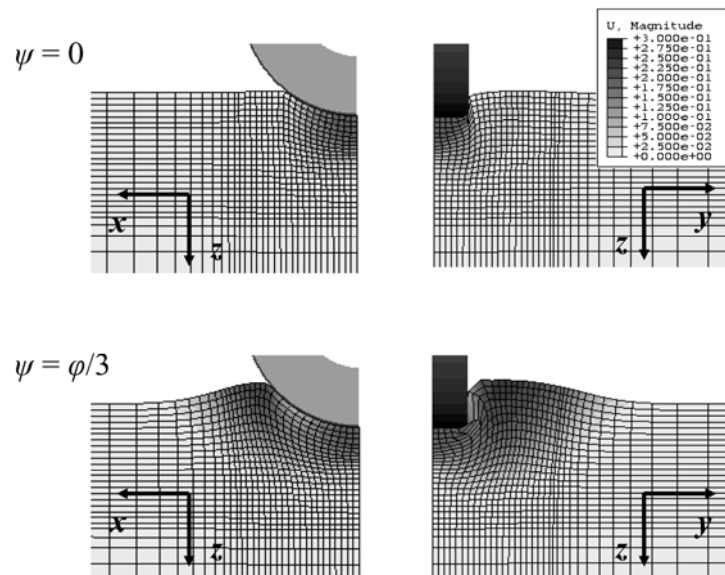


Fig. 3. Effect of dilation angle on kinematics ( $s/d = 0.1$ ,  $b/d = 0.3$ ,  $\varphi = 30^\circ$ ,  $c/\gamma d = 7.2 \times 10^{-2}$ ).



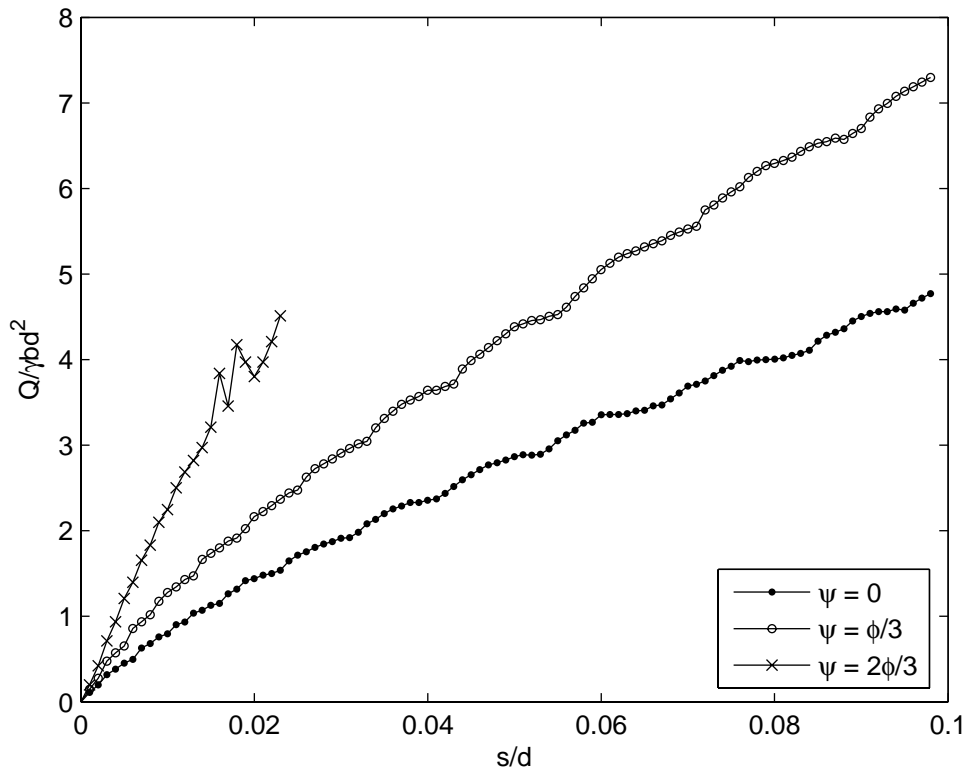


Fig. 4. Effect of dilation angle on indentation force ( $b/d = 0.3$ ,  $\phi = 30^\circ$ ,  $c/\gamma d = 7.2 \times 10^{-2}$ ).

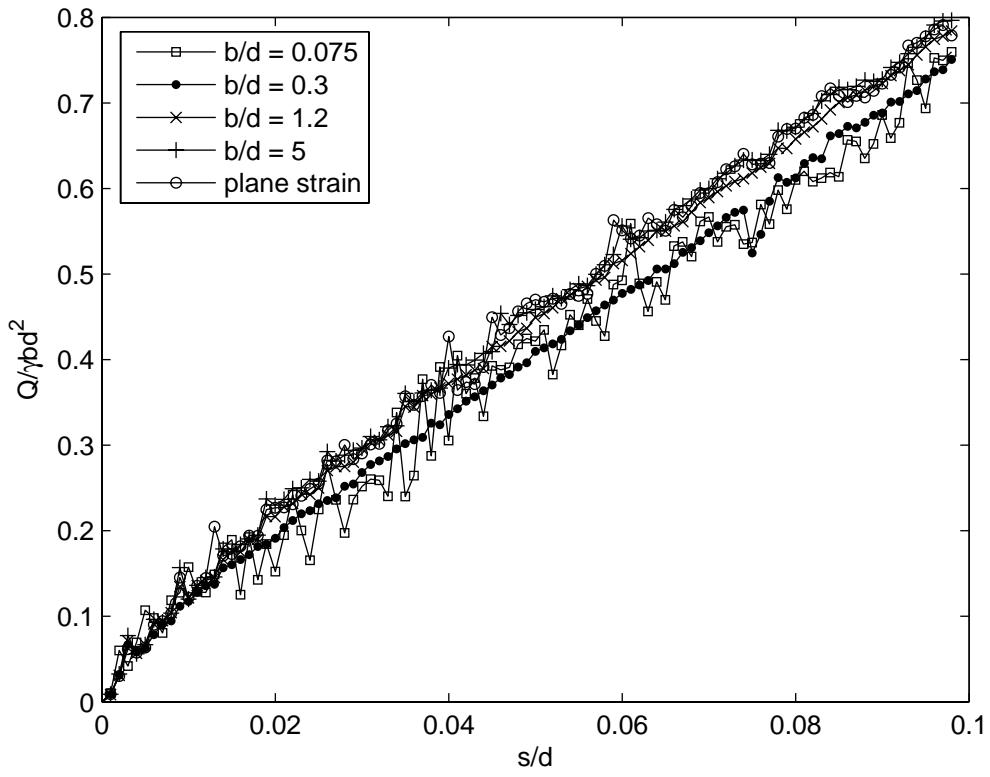


Fig. 5. Indentation force for sand with small friction angle and varying  $b/d$  ( $\varphi = 15^\circ$ ,  $\psi = 0$ ,  $c/\gamma d = 1.25 \times 10^{-2}$ ).

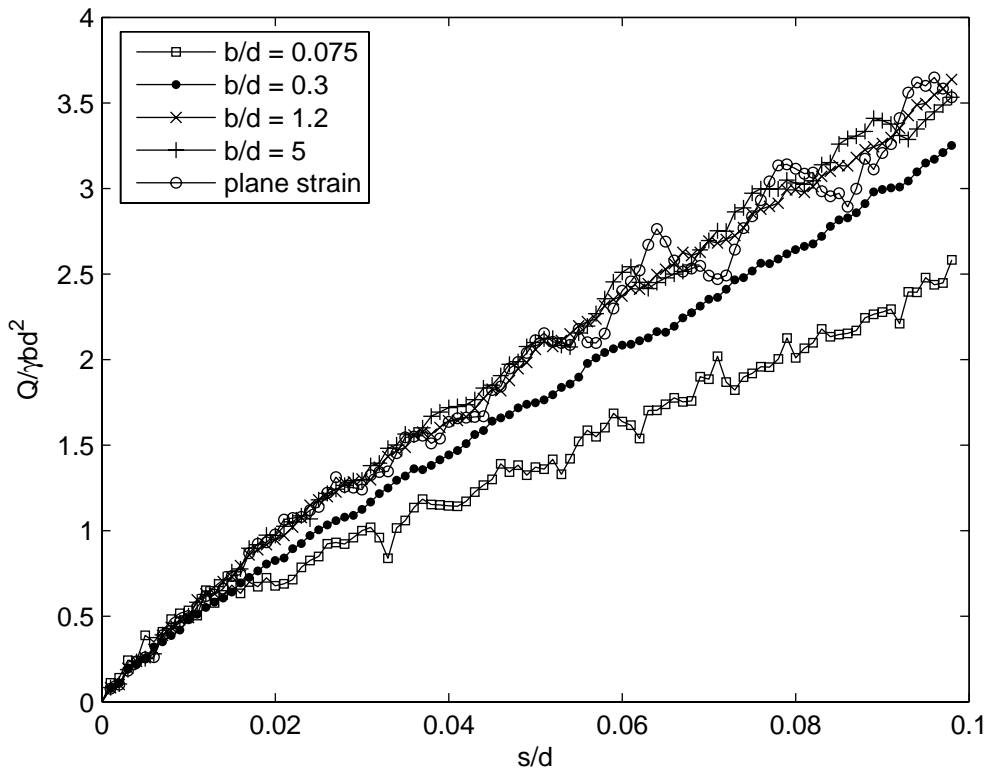


Fig. 6. Indentation force for sand with medium friction angle and varying  $b/d$  ( $\varphi = 30^\circ$ ,  $\psi = 0$ ,  $c/\gamma d = 1.25 \times 10^{-2}$ ).

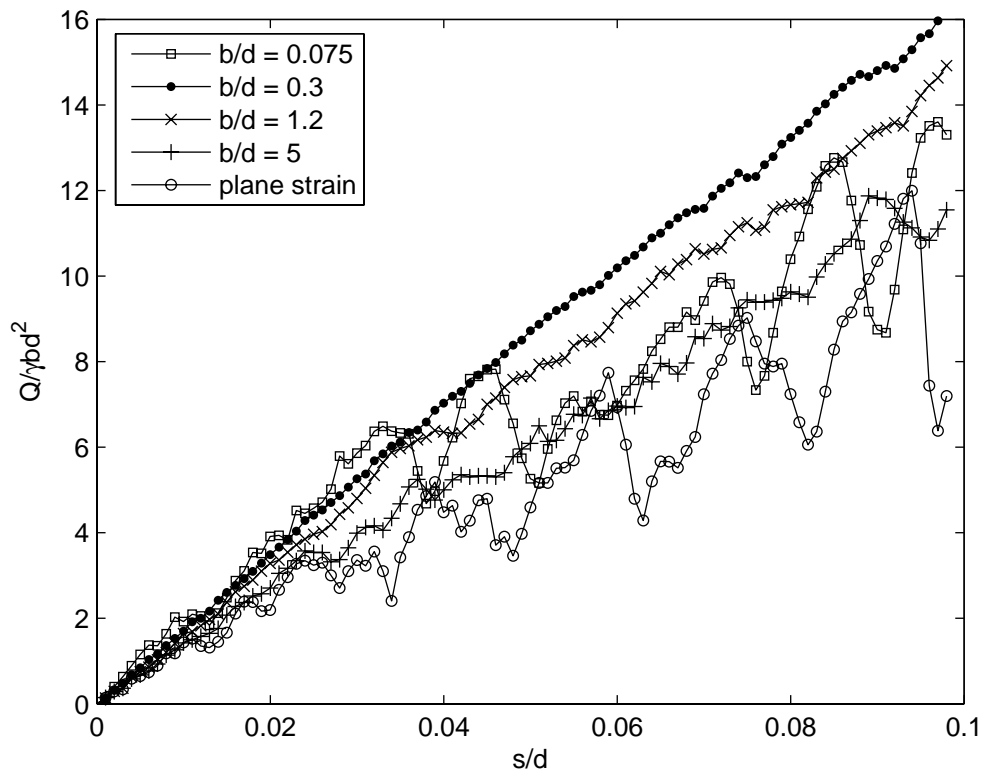


Fig. 7. Indentation force for sand with large friction angle and varying  $b/d$  ( $\varphi = 45^\circ$ ,  $\psi = 0$ ,  $c/\gamma d = 1.25 \times 10^{-2}$ ).

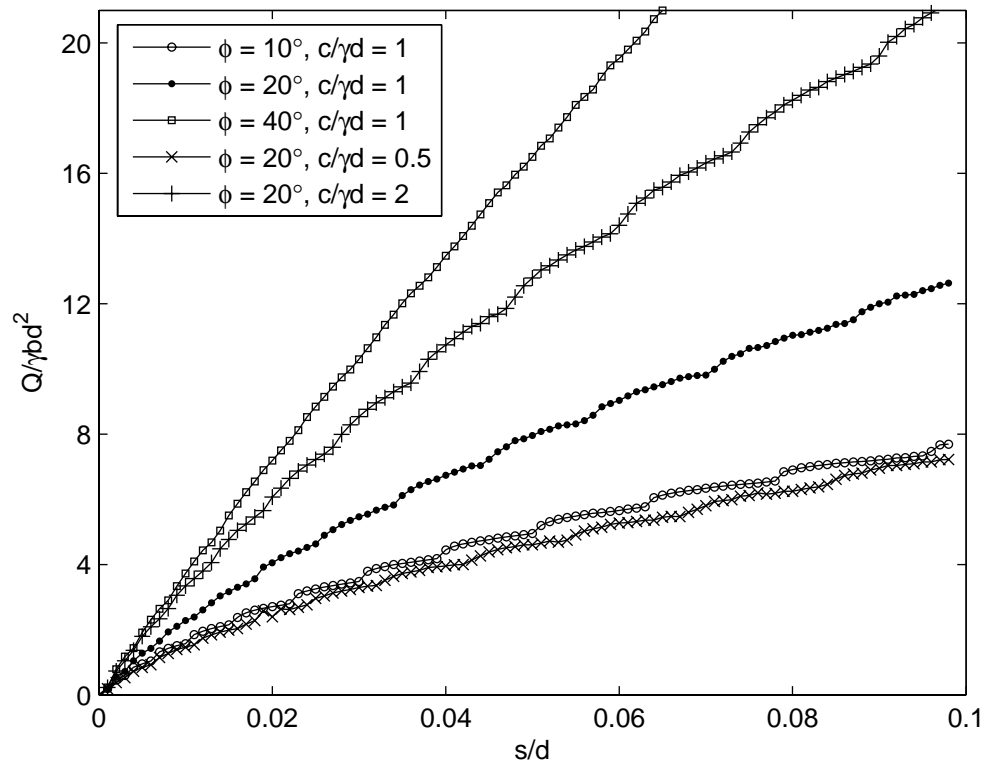


Fig. 8. Influence of  $\phi$  and  $c$  on indentation force ( $\psi = 0, b/d = 0.3$ ).

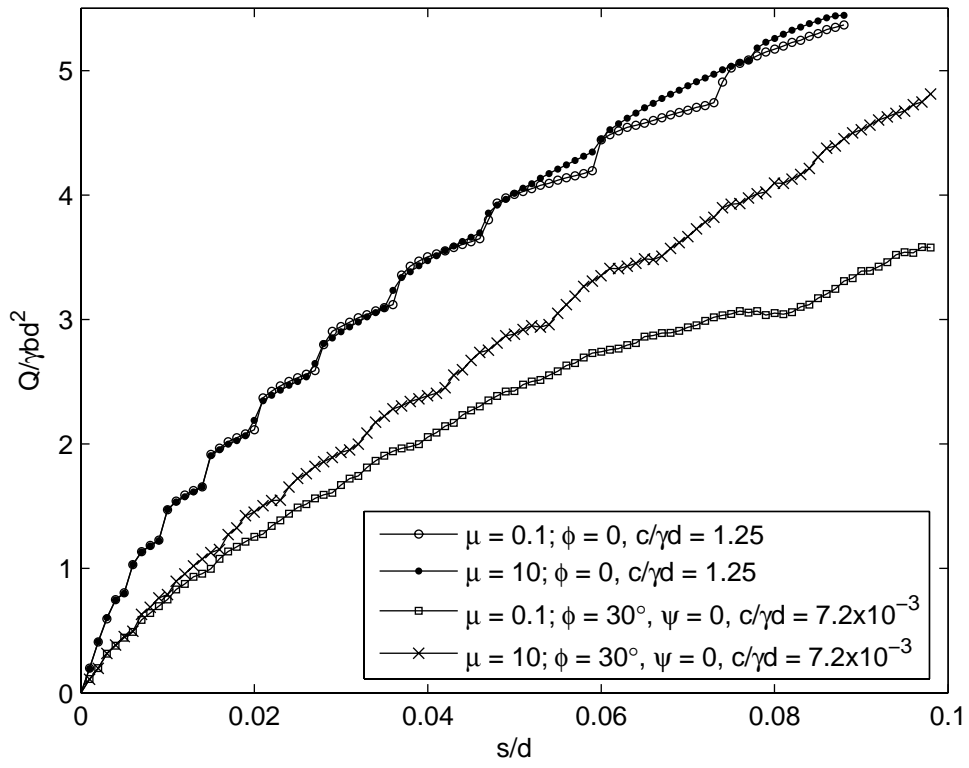


Fig. 9. Effect of interface friction on indentation force ( $b/d = 0.3$ ).

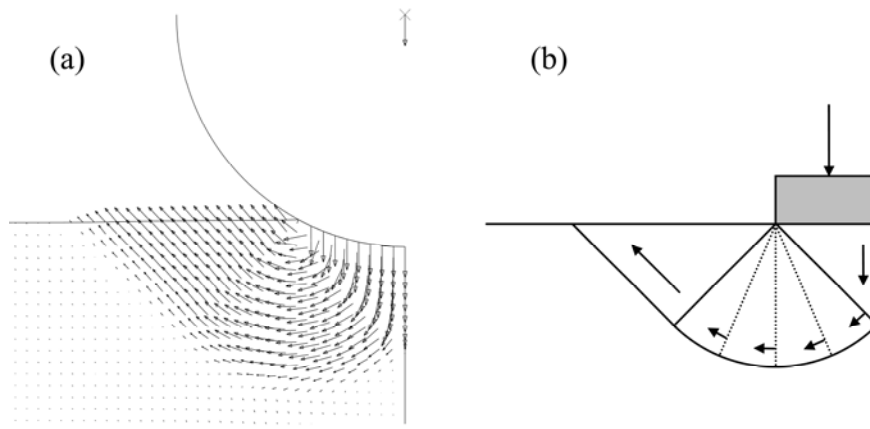


Fig. 10. Incremental displacements for clay soil ( $\phi = 0$ ). (a) ABAQUS; (b) Prandtl solution.

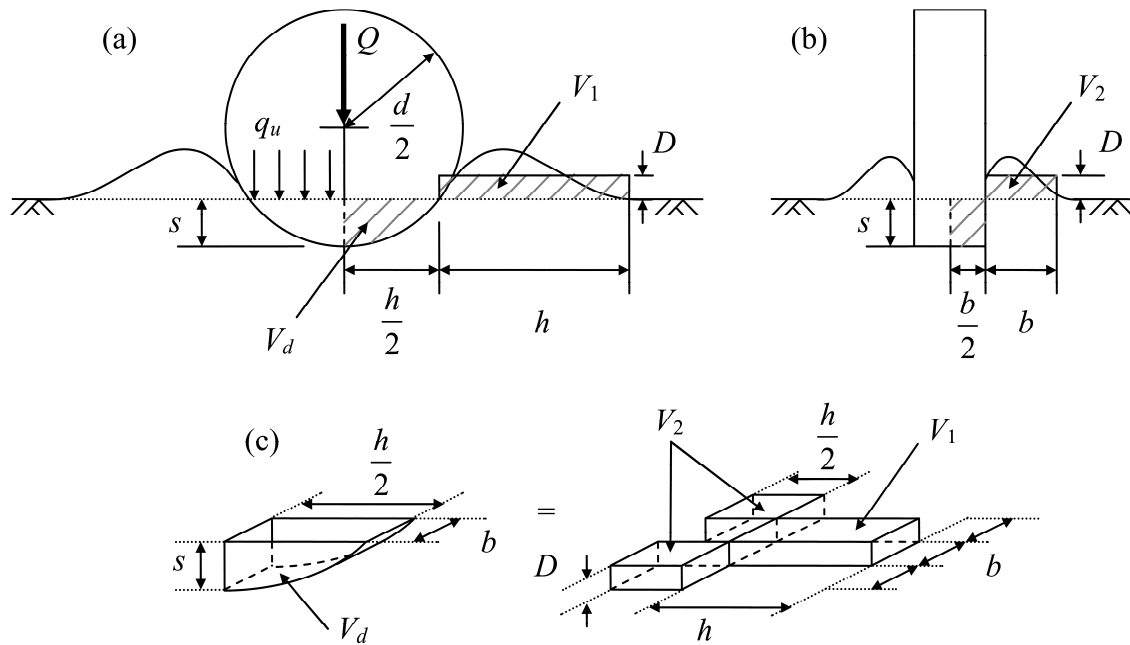


Fig. 11. Wheel indentation as equivalent bearing capacity problem. (a) view in plane of wheel diameter; (b) view in plane of wheel width; (c) assumed geometry of displaced soil for estimation of  $D$  [2].



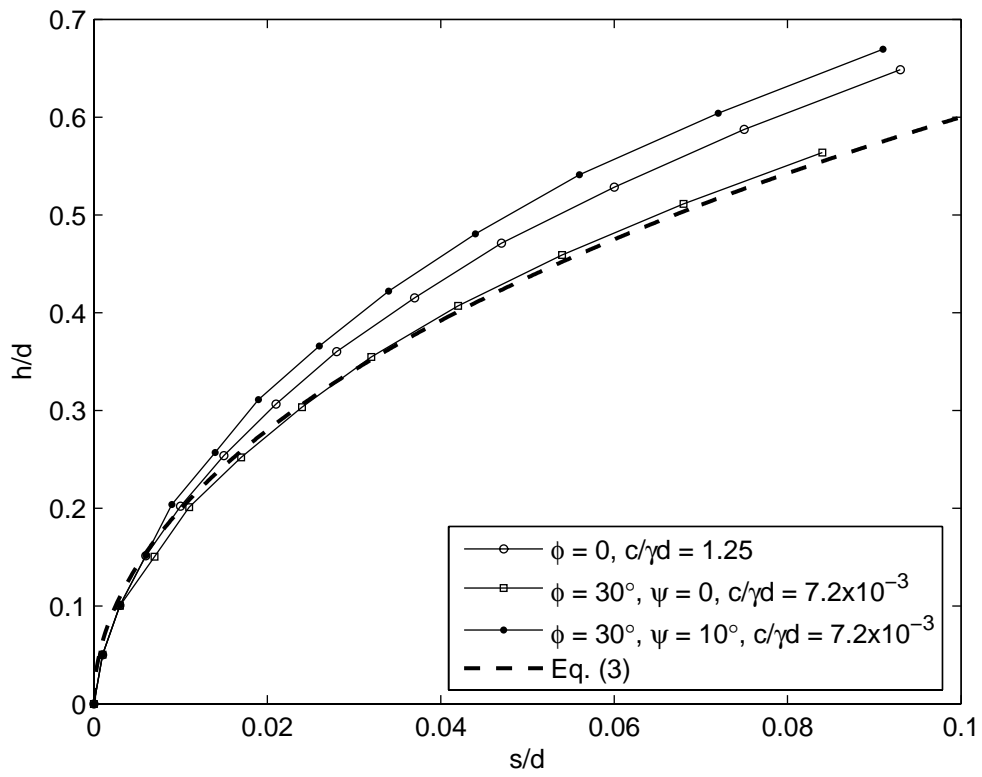


Fig. 12. Contact length in analytic method and numerical simulations ( $b/d = 0.3$ ).

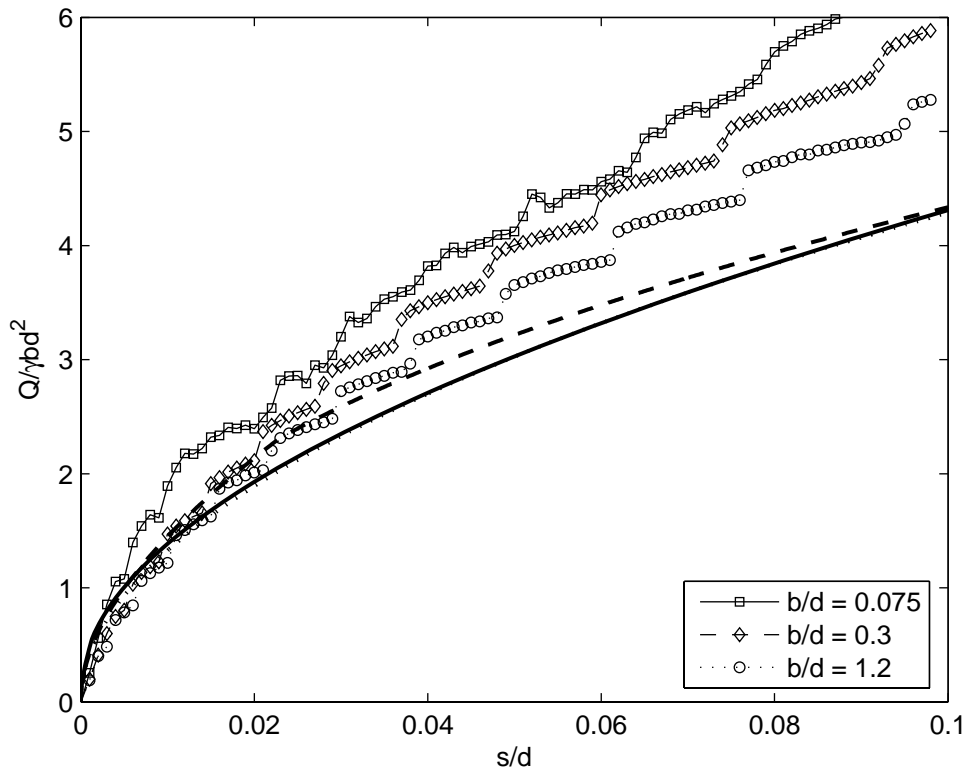


Fig. 13. Comparison of analytic method and numerical simulations for clay ( $\varphi = 0$ ,  $c/\gamma d = 1.25$ , smooth curves are from analytic method, markers are from ABAQUS).

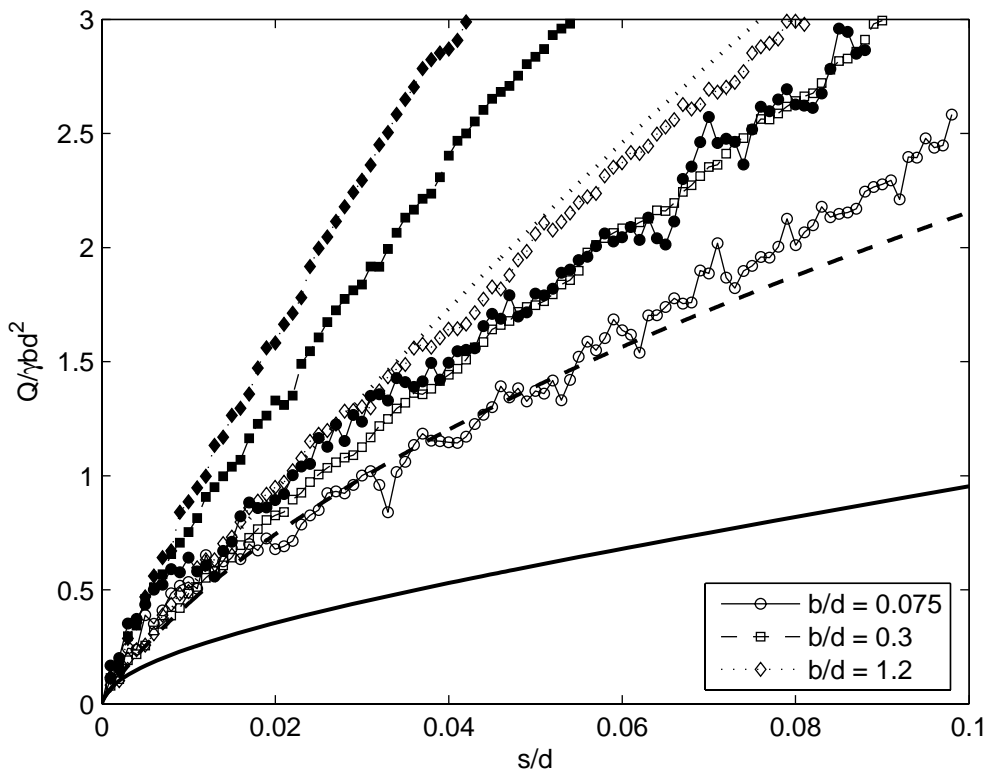


Fig. 14. Comparison of analytic method and numerical simulations for sand with medium friction angle ( $\varphi = 30^\circ$ ,  $c/\gamma d = 1.25 \times 10^{-2}$ , smooth curves are from analytic method, open markers are from ABAQUS with  $\psi = 0$ , filled markers are from ABAQUS with  $\psi = 10^\circ$ ).

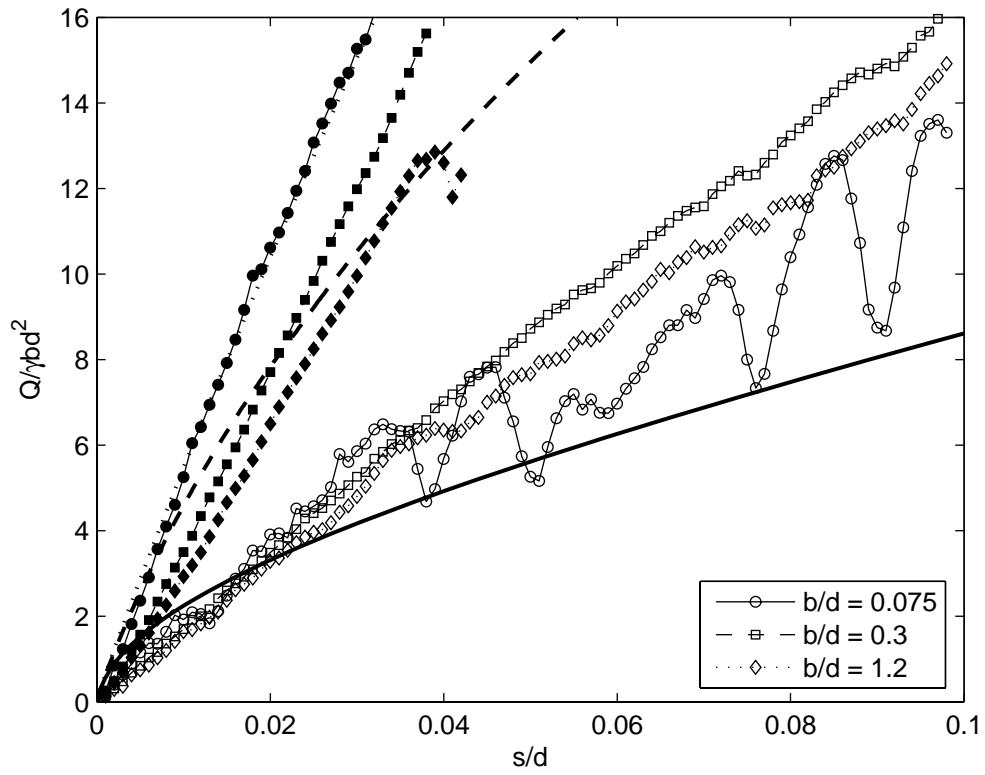


Fig. 15. Comparison of analytic method and numerical simulations for sand with high friction angle ( $\varphi = 45^\circ$ ,  $c/\gamma d = 1.25 \times 10^{-2}$ , smooth curves are from analytic method, open markers are from ABAQUS with  $\psi = 0$ , filled markers are from ABAQUS with  $\psi = 15^\circ$ ).

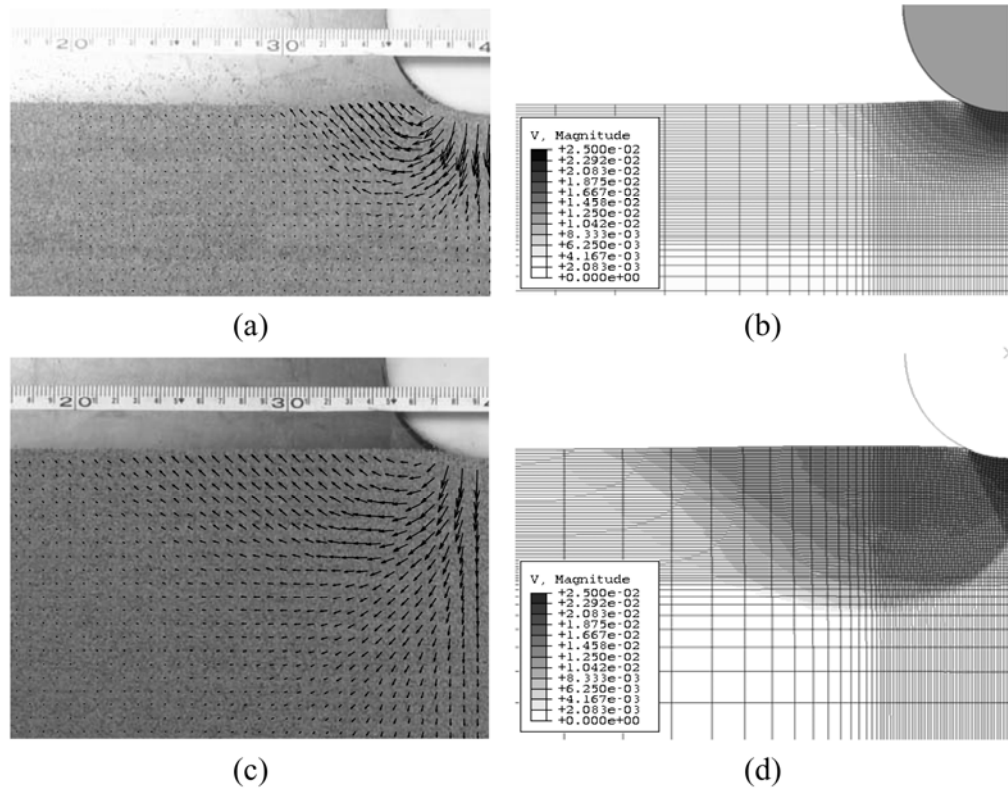


Fig. 16. Displacement increments from PIV and numerical simulations ( $s/d = 0.04$ ,  $\varphi = 40^\circ$ ,  $\psi = 20^\circ$ ). (a) PIV, midplane for  $b/d = 0.38$ ; (b) ABAQUS, midplane for  $b/d = 0.38$ ; (c) PIV, plane strain; (d) ABAQUS, plane strain.

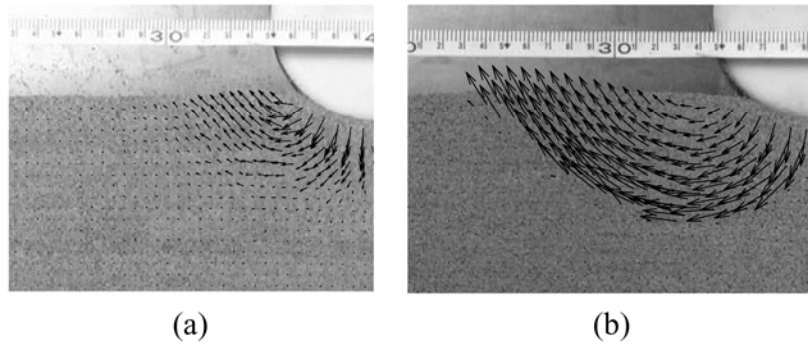


Fig. 17. Displacement increments from PIV ( $s/d = 0.1$ ). (a) midplane for  $b/d = 0.38$ ; (b) plane strain.

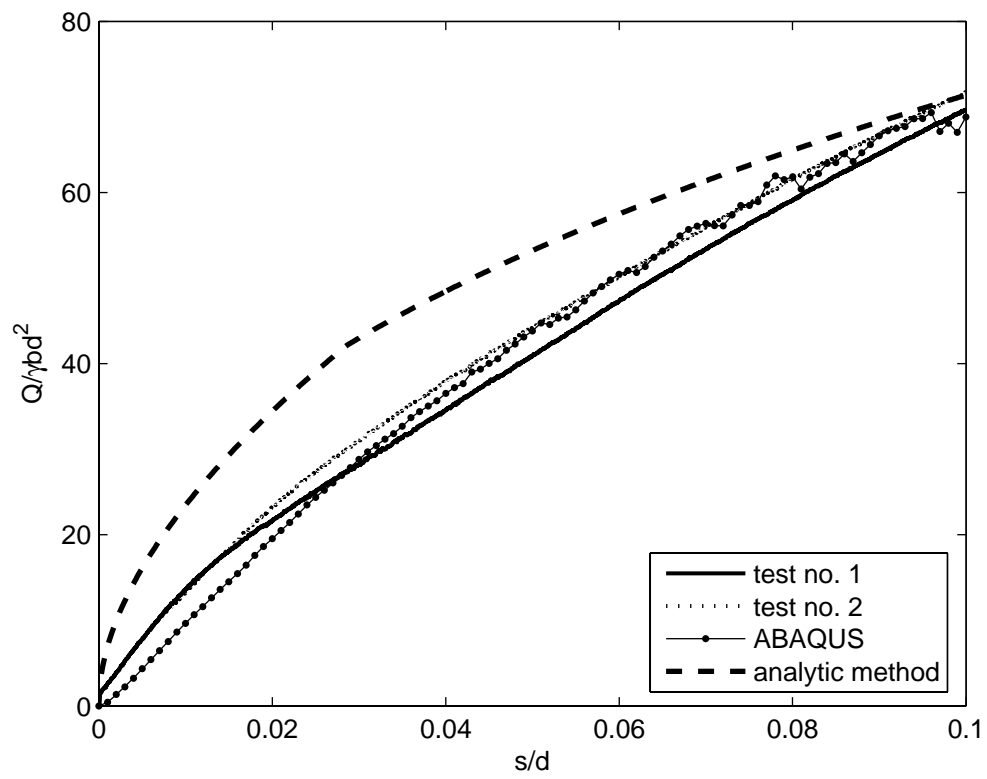


Fig. 18. Comparison of theoretical predictions and experimental data for clay.

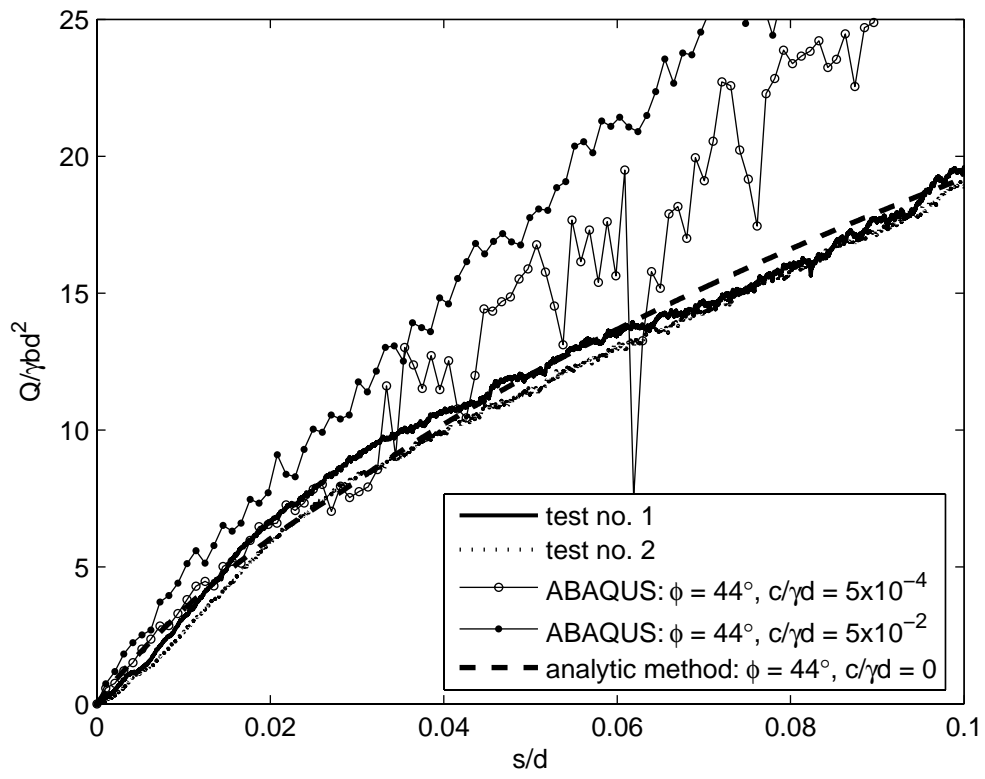


Fig. 19. Comparison of theoretical predictions and experimental data for dense sand.